



HAL
open science

Analysis of the dual function of the ESCRT-III protein Snf7 in endocytic trafficking and in gene expression

Peter Weiss, Stefanie Huppert, Ralf Kölling

► **To cite this version:**

Peter Weiss, Stefanie Huppert, Ralf Kölling. Analysis of the dual function of the ESCRT-III protein Snf7 in endocytic trafficking and in gene expression. *Biochemical Journal*, 2009, 424 (1), pp.89-97. 10.1042/BJ20090957 . hal-00479213

HAL Id: hal-00479213

<https://hal.science/hal-00479213>

Submitted on 30 Apr 2010

HAL is a multi-disciplinary open access archive for the deposit and dissemination of scientific research documents, whether they are published or not. The documents may come from teaching and research institutions in France or abroad, or from public or private research centers.

L'archive ouverte pluridisciplinaire **HAL**, est destinée au dépôt et à la diffusion de documents scientifiques de niveau recherche, publiés ou non, émanant des établissements d'enseignement et de recherche français ou étrangers, des laboratoires publics ou privés.

Analysis of the dual function of the ESCRT-III protein Snf7 in endocytic trafficking and in gene expression

Short title: Dual function of *SNF7*

Keywords: ESCRT, Rim101 pathway, endocytosis, multivesicular body, vacuolar protein sorting, CHMP4

Peter Weiß, Stefanie Huppert and Ralf Kölling¹
Institut für Lebensmittelwissenschaft und Biotechnologie, Fg. Gärungstechnologie,
Universität Hohenheim, D-70599 Stuttgart, Germany

¹Corresponding author:

Ralf Kölling
Institut für Lebensmittelwissenschaft
und Biotechnologie
Fg. Gärungstechnologie (150f)
Universität Hohenheim
Garbenstr. 23
D-70599 Stuttgart
Tel. 0711-459 22310
Fax. 0711-459 24121
email: koelling@uni-hohenheim.de

Synopsis

ESCRT-III mediates budding and scission of intraluminal vesicles into multivesicular endosomes. For the main ESCRT-III subunit Snf7, an additional role in activation of the transcription factor Rim101 ("Rim pathway") is now firmly established. Here, we investigate how the two Snf7 functions are related to each other. By generating *SNF7* mutations that severely affect endocytic trafficking, but leave the Rim pathway function intact, we show that the two functions of *SNF7* can be separated genetically. We analyzed in detail, how the *SNF7* mutations affect the interaction of Snf7 with its various binding partners. While interactions with Rim-related functions (Rim13, Rim20) were not altered by the mutations, there was a strong effect on interactions with components of the ESCRT pathway. The interaction with the ESCRT-III subunits Vps20 and Vps24 was strongly increased by the mutations, while the interaction with functions acting downstream of ESCRT-III (Vps4 and Bro1) was reduced. Since Vps4 is required for disassembly of ESCRT-III, these data suggest that ESCRT-III is more stable in our *SNF7* mutants. In line with this notion, a higher fraction of mutant Snf7 was detected at the membrane. Upon shift to alkaline pH, a stronger binding signal for virtually all interaction partners (except for Vps4) was observed. This indicates that the ESCRT network at the endosomal membrane is more extensive under these conditions.

Introduction

During endocytosis, cell surface proteins are internalized and transported via several endosomal intermediates to the lysosome/vacuole for degradation. Endocytic cargo proteins are marked for degradation by ubiquitination [1]. Ubiquitinated membrane proteins are then recognized by the endocytic machinery and are incorporated into vesicles that bud into the interior of multivesicular endosomes (MVBs). After fusion of the MVB with the lysosome/vacuole, the internal vesicles are released into the lumen of the hydrolytic compartment, where they are degraded.

Cargo recruitment and internal vesicle formation is mediated by ESCRT (endosomal sorting complex required for transport) proteins [2]. These proteins can be grouped into several complexes, ESCRT-0, -I, -II and -III that are thought to act sequentially in cargo recruitment and vesicle formation at the endosomal membrane ("ESCRT pathway"). The ESCRT complexes are released from the endosomal membrane by the AAA-ATPase Vps4 for further rounds of membrane budding [3].

ESCRT-III in conjunction with Vps4 appears to be the "machine" driving internal vesicle formation. The topology of membrane budding mediated by ESCRT-III is unique in that it is directed away from the cytoplasm. Other membrane budding and fusion processes like retrovirus budding [4] and cytokinesis [5, 6] with the same topology also make use of the ESCRT-III machinery. The ESCRT-III/Vps4 machinery for membrane budding and fusion appears to be a very ancient system, since it is also conserved in archaea, where it plays a role in cytokinesis [7].

Yeast ESCRT-III consists of four core subunits Snf7, Vps2/Did4, Vps20 and Vps24 [8] and two "ESCRT-III associated subunits" Did2 [9] and Mos10/Vps60 [10], which are all homologous to each other. Snf7 has the propensity to homo-oligomerize and is the most abundant subunit in the complex. Vps20 induces Snf7 oligomerization, whereas the other core subunits Vps2 and Vps24 seem to limit oligomerization by recruiting Vps4 and inducing disassembly [11].

Filament formation appears to be a general property of ESCRT-III proteins. Upon overexpression of human Snf7 (CHMP4) in mammalian cells, circular arrays of filaments on membranes were observed [12]. Budding and tubulation of membranes away from these

circular scaffolds could be observed upon co-expression of an ATP-hydrolysis deficient VPS4B mutant. Likewise, helical filament formation in vitro has been observed with yeast Vps24 [13] and human CHMP2A [14].

Recently, budding of intraluminal vesicles could be reconstituted in vitro with purified components [15]. It was shown that Vps20, Snf7 and Vps24 were sufficient to detach intraluminal vesicles into giant unilamellar vesicles. Vps2 and Vps4 were required for ESCRT-III recycling and additional rounds of vesicle budding.

Although all ESCRT-III proteins function at the same step in MVB-formation, individual ESCRT mutants also show distinct phenotypes [16], which points to a specific role of ESCRT proteins in gene regulation. It is now firmly established that Snf7 plays a role in activation of the transcription factor Rim101 [17-20]. Under inducing conditions, like shift to alkaline pH, the inactive Rim101 precursor is processed to its active form by C-terminal cleavage [21]. The C-terminally processed transcription factor then moves to the nucleus, where it regulates the expression of specific target genes [22]. We recently showed that the *SUC2* gene coding for the enzyme invertase is also a target of the Rim pathway offering an explanation for the sucrose non-fermenting phenotype of *SNF7* mutants [16].

The current view is that Rim101 cleavage takes place on a platform consisting of Snf7, the Bro1-domain protein Rim20 and the calpain-like protease Rim13 [23]. In addition, Rim101 activation depends on a number of other Rim-functions thought to be involved in pH signalling [24] and on components acting upstream of Snf7 in the ESCRT pathway [17-20]. At present, it is unclear what role the upstream ESCRT functions play in Rim101 activation.

Here, we investigate the connection between the two functions of Snf7 in the ESCRT pathway and in gene expression. We found that the two functions can be separated genetically. We were able to generate Snf7 mutants that are selectively blocked in endocytic trafficking, but that are normal with respect to gene expression. A detailed phenotypic analysis of the Snf7 mutants showed that binding to downstream functions like Vps4 and Bro1 is reduced in the mutants. This suggests that disassembly of ESCRT-III is affected by the Snf7 mutations. We propose that the composition of the ESCRT-III complex may be important for Rim activation.

Experimental

Yeast strains and plasmids

The yeast strains used are listed in Table 1. Yeast cells were grown in SD/CAS medium (0.67 % yeast nitrogen base, 1 % casamino acids, 2 % glucose). In some experiments, 50 mM MOPS was added and the pH was adjusted to pH 3 or pH 7. Deletion strains and strains carrying 13myc-tagged gene variants are derived from the wildtype strain JD52. They were constructed by one-step gene replacement with PCR-generated cassettes [25]. For N-terminal 3HA-tagging of Rim101, the *GAL1* promoter in pFA6a-His3MX6-PGAL1-3HA was replaced by a *RIM101* promoter fragment. The deletions and insertions were verified by PCR. To construct pRK861, a 1843 bp PCR fragment with attached *Bam*HI and *Sal*I sites containing the *SNF7* ORF including the *SNF7* promoter was cloned into YCplac33 [26].

SNF7 mutagenesis

To generate *SNF7* mutations an error-prone PCR reaction was performed. The reaction-mix contained: 2.5 mM MgCl₂, 0.5 mM MnCl₂, 0.5 mM dNTPs, 1 μM primers, 4 U Taq-polymerase, 2 ng pRK861 template DNA. 35 cycles were performed with 1 min annealing at 57.4°C and 4 min elongation at 68°C. The PCR fragments were co-transformed with YCplac33 linearized with *Bam*HI and *Sal*I into the $\Delta snf7 \Delta his3$ strain RKY1854 that carried a *STE6-HIS3* expression cassette integrated into the genome. In the yeast cells, an intact plasmid was regenerated by homologous recombination between the PCR-fragment and

vector sequences. Ste6-His3 was expressed from the *CUP1* promoter thus efficient expression required Cu^{2+} -ions in the growth medium. His⁺ transformants were selected on SD plates containing 0.5 mM CuSO_4 and required auxotrophic markers (but without histidine and uracil). Among 35,000 transformants with intact plasmids, 128 transformants were obtained that were able to grow on -his plates. Among the his⁺ transformants, 20 transformants were found that were wildtype with respect to temperature sensitivity and growth on raffinose.

Co-immunoprecipitation and cell fractionation

Cells were grown over night to exponential phase ($\text{OD}_{600} < 1.5$; $5 \times 10^7/\text{ml}$) in SD/CAS medium. 20 OD_{600} of cells were harvested, washed in cold 10 mM NaN_3 , resuspended in 100 μl lysis-buffer (0.3 M sorbitol, 10 mM NaN_3 , 50 mM HEPES pH 7.5, + protease inhibitors) and lysed by agitation with glass beads for 5 min. After addition of 650 μl of lysis-buffer, samples were incubated with 1 % Triton X-100 on ice for 30 min. Then the cell extracts were centrifuged for 5 min at 500 g to remove cell debris. The supernatant was incubated for 1 h at 4°C with antibody and for another 1 h at 4°C with 50 μl of a protein A-Sepharose beads (20 % suspension). The protein A-beads were washed three times with lysis-buffer in a table top centrifuge (2x 1 min 150 g, 1x 20 s 13,000 g), resuspended in 100 μl SDS gel sample buffer and incubated for 15 min at 50°C before gel loading. For cell fractionation, cell extracts were prepared in the same way, but the incubation with Triton X-100 was omitted. The cleared cell extract was centrifuged at 100,000 g for 1 h at 4°C. The pellet (P100) was resuspended in the original volume of lysis buffer. For subsequent immunoprecipitation, 1 % Triton X-100 was added to the fractions (P100 and S100) and incubated on ice for 30 min. Immunoprecipitation was then further continued as described above.

Preparation of cell extracts for detection of Rim101 processing

Standard cell lysis triggers Rim101 processing. Therefore, the fast-boil lysis protocol was used to assay Rim101 processing. Before harvesting of the cells, 1 mM PMSF was added to the culture. Cells were spun down, resuspended in 100 μl lysis buffer (as above) and immediately heated to 95°C for 5 min. Then, cells were broken by glass bead lysis for 5 min.

Other methods

The pulse-chase, CPY-sorting and flotation experiments were performed as described previously [10, 27, 28].

Results

Separation of *snf7* phenotypes by mutagenesis

All of the Snf7 homologues appear to be involved in the formation of multivesicular bodies (MVBs) at late endosomes, yet deletion mutants display distinct phenotypes [16]. These distinct phenotypes could reflect a particular function at endosomes, like e.g. recruitment of specific cargo proteins for vacuolar degradation. Alternatively, they could point to additional functions for the Snf7 homologues completely unrelated to their endosomal function. If the observed phenotypes of the deletion mutants (sensitivity to high temperature, caffeine and congo red, poor growth on raffinose) are unrelated to their endosomal function, it should be possible to separate these functions genetically from the endosomal function.

To test this prediction, we looked for *SNF7* mutants that are blocked in the endocytic pathway but that are wildtype with respect to the other phenotypes. To be able to detect a block in the endocytic pathway, we made use of the α -factor transporter Ste6. We have shown previously that Ste6 is a short-lived protein that is transported via the endocytic pathway to the vacuole where it is degraded [28]. In Δsnf7 mutants, Ste6 is stabilized because its transport to the vacuole is blocked [10]. To facilitate detection of Ste6, it was fused to the marker protein

His3 that is required for histidine synthesis. Under normal conditions, due to the high turnover of the fusion protein, the amount of Ste6-His3 is not high enough to promote growth of a $\Delta his3$ strain on media lacking histidine. However, when Ste6-His3 is stabilized, like in the $\Delta snf7$ mutant, Ste6-His3 accumulates to higher levels and thus provides sufficient His3 activity to enable the $\Delta his3$ strain to grow.

SNF7 mutants were generated by error-prone PCR. Among the his⁺ transformants, 20 transformants were found that were wildtype with respect to temperature sensitivity and growth on raffinose (examples are shown in Fig. 1A). This demonstrates that it is indeed possible to genetically separate the different Snf7 functions. Sequencing of 12 mutant genes revealed that most *SNF7* genes carry multiple mutations (Tab. 2). Some of the mutations are probably irrelevant to the phenotype. Still, the distribution of the mutations was quite uneven. They clustered in the N-terminal half of Snf7 and at its very C-terminus (Fig. 1B). There is structural information available for one ESCRT-III protein, for human CHMP3, the homologue of yeast Vps24 [29]. Since all ESCRT-III proteins appear to have a similar structure, the Snf7 mutations can be modeled onto the 3D-structure of CHMP3. The CHMP3 core structure consists of a four-helical bundle with two long helices ($\alpha 1$, $\alpha 2$) forming a 70 Å hairpin structure and two additional short helices ($\alpha 3$, $\alpha 4$) across the $\alpha 1$ - $\alpha 2$ hairpin. A fifth helix ($\alpha 5$) is connected to the core by a largely disordered linker and an additional sixth, C-terminal helix ($\alpha 6$) is not represented in the structure (Fig. 1C). Hydrophobic amino acids show a heptad-repeat pattern in helices $\alpha 2$ and $\alpha 6$. Chances are therefore high that these helices are engaged in coiled-coil interactions.

Our Snf7 mutations cluster in the N-terminal half of Snf7 comprising the $\alpha 1$ - $\alpha 3$ region and in $\alpha 6$. Thus, these regions appear to be important for the endosomal function of Snf7. Since the region between $\alpha 3$ and $\alpha 6$ is largely devoid of mutations and since we selected for mutants that retain the gene expression function, one may conclude that this region is crucial for the gene expression function of Snf7. Two Snf7 mutants with single mutations (M3: L26W and M5: S93P) were selected for further analysis (Fig. 1C).

To exclude that the higher His3-activity in the *snf7* mutants was simply due to higher *STE6-HIS3* expression, the Ste6 half-life was determined by pulse-chase experiments in the $\Delta snf7$ strain transformed with different *SNF7* mutant plasmids (Fig. 2A). Ste6 was turned over rapidly with wildtype *SNF7* (half-life 21 min) and was stabilized about 5-fold with the vector control ($\Delta snf7$), as reported previously [10]. Similarly, Ste6 was stabilized 2- to 3-fold with the mutant *SNF7* variants. This demonstrates that the observed His⁺ phenotype of the *SNF7* mutants is indeed due to stabilization of Ste6-His3.

To further prove a Ste6 trafficking defect, the intracellular distribution of a Ste6-GFP fusionprotein was examined in the mutants (Fig. 2B). Due to high turnover of Ste6-GFP, only a faint staining of the vacuolar lumen is observed in a wildtype strain. The $\Delta snf7$ mutant, in contrast, showed a typical "class E" staining pattern [30], i.e. a brightly staining dot close to the vacuole with some faint staining of the vacuolar membrane. In line with a Ste6 trafficking defect, our *SNF7* mutants M3 and M5 showed a class E phenotype indistinguishable from $\Delta snf7$.

To exclude that the *SNF7* defects are restricted to Ste6 turnover, we also examined the trafficking of another protein, carboxypeptidase Y (CPY), which passes through endosomes on its way to the vacuole. By passing from one compartment to the other, CPY receives different modifications that can be distinguished by gel mobility. In the endoplasmic reticulum, it is core-glycosylated to the p1-form, in the Golgi it is converted into the slower migrating, outer-chain glycosylated p2-form and in the vacuole the mature m-form is finally generated by proteolytic cleavage of the precursor. In vacuolar protein sorting (*vps*) mutants, which are defective in endosomal transport, p2-CPY is missorted to the culture medium. To detect missorting, CPY was immunoprecipitated from cell extracts and from culture supernatants. CPY sorting was examined by a pulse-chase experiment (Fig. 2C). Shortly after

pulse labeling (t_0), all three CPY forms can be detected in the internal fraction. After a 40 min chase period in the wildtype strain, CPY is completely converted to the m-CPY form, which is exclusively found in the internal fraction. In contrast, a certain fraction of p2-CPY is detected in the culture medium of the $\Delta snf7$ mutant. In this respect, our *SNF7* mutants (M3, M5) behaved like the $\Delta snf7$ deletion mutant. This demonstrates that our *SNF7* mutants have a general defect in endosomal trafficking.

Snf7 is required for the activation of the transcription factor Rim101 ("Rim pathway"). We were specifically interested whether our *Snf7* mutants interfere with the activity of the Rim pathway. Therefore, several aspects of Rim pathway function were assayed in our mutants. First, the induction of invertase after shift from high to low glucose medium was examined. We have shown recently that the invertase gene *SUC2* is a target of the Rim pathway and that active Rim101 is required for high-level expression of invertase [16]. Expression of invertase from the *SUC2* gene is subjected to glucose repression. Two hours after shift to low glucose, the $\Delta snf7$ mutant showed a much lower invertase activity than wildtype (about 30 %) whereas our *SNF7* mutants (M3, M5) displayed wildtype activity (Fig. 3A). This result might have been already expected from the fact that our mutants show wildtype growth on raffinose media (Fig. 1A), since raffinose is an invertase substrate.

Another *rim* phenotype is sensitivity to lithium chloride [23]. To test for lithium sensitivity, serial dilutions of cultures were spotted onto plates containing 0.3 M LiCl. As can be seen in Fig. 3B, the $\Delta snf7$ strain is just as sensitive to LiCl as the Rim pathway mutant $\Delta rim13$. Our mutants M3 and M5, however, grow like wildtype and are not affected by LiCl.

Upon shift to alkaline pH, Rim101 is activated by proteolytic cleavage [23], presumably mediated by the calpain-like protease Rim13 giving rise to a spectrum of bands, rather than to a single cleavage product. As expected, no cleavage was observed in the $\Delta rim13$ and $\Delta snf7$ mutants, upon shift from pH 3 to pH 7 (inducing conditions) (Fig. 3C). In contrast, cleavage indistinguishable from wildtype was seen with the M3 and M5 mutants.

Taken together, our experiments clearly show that protein trafficking in the endocytic pathway is severely affected by our *SNF7* mutations, while Rim pathway function is completely normal in the mutants. Thus, our mutations selectively affect the endocytic function of *Snf7*, while leaving the Rim pathway function intact.

Membrane association of *Snf7* mutants

To further characterize the nature of the endosomal defect of our *SNF7* mutants, the mutant *Snf7* variants were examined for membrane association. It has been shown previously that *Snf7* associates with endosomal membranes as part of the ESCRT-III complex [8]. Since the membrane-associated fraction of *Snf7* is higher in *vps4* mutants [3], these experiments were performed in a $\Delta vps4 \Delta snf7$ background. Membrane association was examined by flotation on OptiprepTM-gradients. During centrifugation membranes float to the top of the gradient due to their low density while proteins not attached to membranes remain behind in the lower, denser fractions of the gradient. Six fractions were collected from the gradients. As shown in Fig. 4, the membrane proteins Pep12 (an endosomal SNARE protein) and Pma1 (the plasma membrane ATPase) were mostly found in fraction 1 and 2 of the gradient while the soluble phosphofructokinase (PFK) was mainly found in fractions 4-6. About 60 % of wildtype *Snf7* protein turned out to be membrane associated (fraction 1-3). For mutants M3 and M5, a similar fraction of protein was observed at the membrane. This shows that membrane association is not disrupted by our mutations.

Effect of mutations on *Snf7* interactions

To understand the molecular basis of the selective trafficking defect of the *Snf7* mutations, we analyzed the effect of the mutations on *Snf7* interactions. Evidence has been presented for the existence of *Snf7* filaments [12, 13]. To examine the effect of our mutations on possible

multimer formation, cross-linking experiments were performed. Cell extracts were treated with different concentrations of the non-cleavable cross-linker DSS and were then analyzed by SDS-PAGE and Western blotting with anti-Snf7 antibodies. Upon addition of cross-linker, a regular pattern of anti-Snf7 reactive bands was observed (Fig. 5). In contrast to Snf7, only a single, monomeric band was observed for the ESCRT-III associated protein Mos10/Vps60 (not shown). The observed bands were evenly spaced. The apparent sizes of the protein species were multiples of 38 kDa (38, 75, 110, 160 kDa), which corresponds to the apparent size of monomeric Snf7 on our SDS-PAGE gels. Only one cross-link of 55 kDa did not fit this pattern and could correspond to a cross-link between Snf7 and another protein. In any case, no difference in the cross-linking pattern was observed between wildtype and mutant Snf7 indicating that multimer-formation is not affected by our mutations.

We then examined the interaction with other binding partners by co-immunoprecipitation. The 13myc-tagged binding partners were immunoprecipitated from cell extracts with anti-myc antibodies and the immunoprecipitates were then analyzed by Western blotting with Snf7 antibodies (Fig. 6 and Tab. 3). The homomeric Snf7-Snf7 interaction could be confirmed by co-immunoprecipitation. Again, this interaction was unaffected by our Snf7 mutations. Likewise, no significant effect on Co-IP efficiencies was observed for Rim13 and Rim20. However, a clear effect was observed on Vps20, Vps24, Vps4 and Bro1 Co-IP efficiencies. The Vps20 and Vps24 Co-IP signals were strongly enhanced in the mutants, while the Vps4 and Bro1 signals were significantly reduced. Since Vps4 is required for disassembly of ESCRT-III and since interaction between the mutant Snf7 proteins and Vps4 is reduced, our results suggest that the Snf7 mutations interfere with disassembly of ESCRT-III at the endosomal membrane, which would offer an explanation for the observed *vps*-defect.

If this interpretation is correct, we would expect to see more mutant Snf7 protein at the membrane. To test this prediction, cell extracts were centrifuged at 100,000 g to pellet the membranes and the portion of Vps20 and Snf7 in the pellet fractions was determined (Fig. 7, Tab. 4). With wildtype, 33 % of Vps20 and 14 % of Snf7 were detected in the membrane fraction. In the mutants, the fraction of Vps20 at the membrane was slightly increased compared to wildtype (+30-40 %). The fraction of mutant Snf7 at the membrane, however, was twice as high in the mutants as in wildtype. This is in line with the interpretation that there is more ESCRT-III at the endosomal membrane due to less efficient disassembly. With Vps20, we only observed a moderate increase in membrane association in the mutants. The reason for this moderate effect could be that a large portion of Vps20 is already associated with the endosomal membrane independent of ESCRT-III. In fact, the myristoylated Vps20 appears to have an intrinsic ability to associate with membranes and plays an important role in recruiting the other members of ESCRT-III [8].

We made the assumption that the observed interactions between Snf7 and its binding partners take place at the endosomal membrane. There is evidence that soluble, monomeric ESCRT-III proteins are in a closed conformation preventing homo- or heterotypic ESCRT interactions [31]. Theoretically, our Snf7 mutations could alter the equilibrium between open and closed conformation. Under these conditions, Snf7 interactions may also occur in the soluble phase. To address this point, Vps20 was immunoprecipitated from the P100 and S100 fractions and assayed for Snf7 co-immunoprecipitation (Fig. 7). For wildtype Snf7, as well as for the mutant Snf7 variants, Co-IP signals could only be detected with Vps20 from the P100 fraction. This indicates that the interactions indeed occur at the endosomal membrane.

Effect of pH on Snf7 interactions

The Rim-pathway is activated by alkaline pH [24]. We were therefore interested to see how the Snf7 interactions are affected by pH shift. Snf7 Co-IP efficiencies were determined from cells grown at pH 3 and from cells shifted to pH 7 for 30 min. Again, 13myc-tagged binding partners were immunoprecipitated from cell extracts with anti-myc antibodies and the

immunoprecipitates were analyzed by Western blotting with Snf7 antibodies (Fig. 8). From these experiments, it was obvious that with most binding partners (Rim13, Rim20, Vps20, Bro1) considerably more Snf7 could be co-precipitated at alkaline pH than at pH 3. The notable exception, however, was Vps4 where Co-IP efficiencies were not altered by pH shift. This suggests that the ESCRT-III network at the endosomal membrane is more extensive at alkaline pH offering more binding sites for Snf7 interactors.

Discussion

In this report, we explore the relationship between the function of Snf7 in the ESCRT pathway and in the activation of the transcription factor Rim101. Basically, the question is whether these Snf7 activities are different manifestations of a common function or whether they are separate from each other. In the latter case, it should be possible to obtain *SNF7* mutants that are selectively disrupted in one of the functions. Indeed, we succeeded in isolating *SNF7* mutants that are defective in endocytic trafficking but that are wildtype for Rim101 activity. This indicates that activation of Rim101 is not a mere side effect of ongoing endocytic trafficking, but that it is a distinct activity of Snf7. Whether our mutations cleanly separate the two functions of Snf7 is less clear. The trafficking defect of our point mutants is less severe than the defect of the *SNF7* deletion. Thus, our Snf7 mutants appear to retain some residual activity. While this small residual activity is not sufficient for efficient endocytic trafficking, it may still be adequate for activation of Rim101. But in any case, our data show that the requirements for endocytic trafficking and for Rim101 activation are different.

The Snf7 activities cannot be completely independent from each other, since ESCRT and Rim pathway share the requirement for ESCRT functions acting "upstream" of Snf7 [17-20]. But, if ESCRT and Rim pathways are connected, then how can the selective defect of the Snf7 mutants on endocytic trafficking be explained? To gain mechanistic insight into the coordination of ESCRT and Rim pathways, a detailed phenotypic analysis of our Snf7 mutants was performed. To fulfill its function in MVB formation, Snf7 has to be recruited to the endosomal membrane. We found that membrane association was not affected in our mutants, thus all upstream events leading to membrane recruitment of Snf7 appear to be normal in the mutants. Again, this serves as a hint that Snf7 membrane association is a prerequisite for both activities.

To find out what actually distinguishes our Snf7 mutants from the wildtype protein, we examined the interactions with known binding partners. Basically, the mutations had no effect on Rim13, Rim20 and Snf7 homotypic interactions. But, a clear effect was observed on Vps20, Vps24, Vps4 and Bro1 interactions. The Vps20 and Vps24 Co-IP signals were strongly increased in the mutants, while at the same time the Vps4 and Bro1 signals were significantly reduced. Since Vps4 is required for disassembly of ESCRT complexes at the endosomal membrane and since Vps4 binding is reduced in the mutants, we assume that the mutants are defective in disassembly of ESCRT-III complexes at the endosomal membrane. This appears to be a perfect solution to the demands of our genetic screen: Through the block in ESCRT-III disassembly endocytic trafficking is blocked, while the ESCRT network at the endosomal membrane is preserved for activation of the Rim pathway.

The exact composition of ESCRT-III in our *SNF7* mutants is unclear. The ESCRT-III core subunits do not appear to occur in an equimolar ratio in the complex. The stoichiometry of the complex in yeast has been estimated to be 1:10:5:3 (Vps20:Snf7:Vps24:Vps2) [32]. Thus, Snf7 is the most important and most abundant subunit of the complex. It appears that the other ESCRT-III subunits rather serve a more regulatory role. For instance, binding of the Vps2-Vps24 subcomplex limits the size of the complex and promotes disassembly of ESCRT-III by recruiting Vps4, whereas Vps20 promotes Snf7 oligomerization [32]. In our study, we found that the Co-IP efficiencies between Snf7 and the ESCRT-III subunits Vps20

and Vps24 are much higher with the mutant Snf7 variants than with wildtype Snf7. This finding could be explained in two ways: either the stoichiometry of the ESCRT-III complex is altered in the *SNF7* mutants, i.e. the number of Vps20 and Vps24 subunits in the complex is higher than under wildtype conditions, or the ESCRT-III complexes are more stable leading to a higher steady-state concentration of complexes at the membrane. Maybe, we see a combination of both effects. In our mutants, we detect twice as much Snf7 in the membrane fraction, in line with a higher steady-state concentration of ESCRT-III complexes at the membrane. Yet, Co-IP efficiencies with Vps20 and Vps24 are increased four-fold, which cannot be simply explained by a two-fold increase in the number of complexes at the endosomal membrane.

Our Snf7 mutations M3 (L26W) and M5 (S93P) are localized to helices $\alpha 1$ and $\alpha 2$. These regions have been implicated in homo- and heterotypic ESCRT-III interactions [29]. The higher Co-IP efficiencies of mutant Snf7 with Vps20 and Vps24 could thus be explained in part by tighter binding of these ESCRT-III subunits to helices $\alpha 1$ and $\alpha 2$. However, Vps4 and Bro1 are not likely to bind to the $\alpha 1$ - $\alpha 2$ region. Binding sites for Vps4 or Alix, the mammalian Bro1 homologue, have been mapped to C-terminal regions of ESCRT-III proteins [33-35]. Still, our $\alpha 1$ - $\alpha 2$ mutants show reduced interaction with Vps4 and Bro1. One explanation for these findings is that conformational changes in the $\alpha 1$ - $\alpha 2$ region are conveyed to the C-terminal region of Snf7 and alter the binding affinities for Vps4 and Bro1. Binding of ESCRT-III subunits to the $\alpha 1$ - $\alpha 2$ region could thus modulate Vps4 and Bro1 binding to Snf7. This could be part of the normal functional cycle of ESCRT-III assembly and disassembly. An alternative view would be that our $\alpha 1$ - $\alpha 2$ mutants are locked in a functional state that precludes Vps4 and Bro1 binding. For instance, due to the special structure of the ESCRT-III complex, the binding sites for Vps4 and Bro1 may not be accessible.

Our data suggest that the Snf7 interactions are very sensitive to conformational changes in Snf7. The composition and stability of ESCRT-III could thus be a prime target for metabolic control. It appears that extensive ESCRT network formation at the endosomal membrane is also a prerequisite for Rim pathway activation. In line with this notion, we observed a stronger binding signal for virtually all interaction partners (Rim specific and ESCRT specific) upon shift to alkaline pH, with one notable exception: Vps4, whose binding signal was not affected by pH. This view is further supported by the findings of Hayashi et al. [17] who showed that the Rim pathway is constitutively active when disassembly of the ESCRT complexes is blocked by mutating *DID2*, *VPS24* or *VPS4*. A change in the stability or composition of ESCRT-III may thus be crucial for Rim pathway activation.

Acknowledgements

We are grateful to Karin Krapka for her assistance with some of the experiments. This work was supported by the DFG Ko 963/5-2.

References

- 1 Hicke, L. and Dunn, R. (2003) Regulation of membrane protein transport by ubiquitin and ubiquitin-binding proteins. *Annu. Rev. Cell Dev Biol.* **19**, 141-172
- 2 Saksena, S., Sun, J., Chu, T. and Emr, S. D. (2007) ESCRTing proteins in the endocytic pathway. *Trends Biochem. Sci.* **32**, 561-573
- 3 Babst, M., Wendland, B., Estepa, E. J. and Emr, S. D. (1998) The Vps4p AAA ATPase regulates membrane association of a Vps protein complex required for normal endosome function. *EMBO J.* **17**, 2982-2993
- 4 Morita, E. and Sundquist, W. I. (2004) Retrovirus budding. *Annu. Rev. Cell Dev Biol.* **20**, 395-425

- 5 Morita, E., Sandrin, V., Chung, H. Y., Morham, S. G., Gygi, S. P., Rodesch, C. K. and Sundquist, W. I. (2007) Human ESCRT and ALIX proteins interact with proteins of the midbody and function in cytokinesis. *EMBO J.* **26**, 4215-4227
- 6 Carlton, J. G. and Martin-Serrano, J. (2007) Parallels between cytokinesis and retroviral budding: a role for the ESCRT machinery. *Science.* **316**, 1908-1912
- 7 Samson, R. Y., Obita, T., Freund, S. M., Williams, R. L. and Bell, S. D. (2008) A role for the ESCRT system in cell division in archaea. *Science.* **322**, 1710-1703
- 8 Babst, M., Katzmann, D. J., Estepa-Sabal, E. J., Meerloo, T. and Emr, S. D. (2002) ESCRT-III: an endosome-associated heterooligomeric protein complex required for MVB sorting. *Dev Cell.* **3**, 271-282
- 9 Amerik, A. Y., Nowak, J., Swaminathan, S. and Hochstrasser, M. (2000) The Doa4 deubiquitinating enzyme is functionally linked to the vacuolar protein-sorting and endocytic pathways. *Mol. Biol. Cell.* **11**, 3365-3380
- 10 Kranz, A., Kinner, A. and Kölling, R. (2001) A family of small coiled-coil-forming proteins functioning at the late endosome in yeast. *Mol. Biol. Cell.* **12**, 711-723
- 11 Teis, D., Saksena, S. and Emr, S. D. (2008) Ordered assembly of the ESCRT-III complex on endosomes is required to sequester cargo during MVB formation. *Dev Cell.* **15**, 578-589
- 12 Hanson, P. I., Roth, R., Lin, Y. and Heuser, J. E. (2008) Plasma membrane deformation by circular arrays of ESCRT-III protein filaments. *J. Cell Biol.* **180**, 389-402
- 13 Ghazi-Tabatabai, S., Saksena, S., Short, J. M., Pobbati, A. V., Veprintsev, D. B., Crowther, R. A., Emr, S. D., Egelman, E. H. and Williams, R. L. (2008) Structure and disassembly of filaments formed by the ESCRT-III subunit Vps24. *Structure.* **16**, 1345-1356
- 14 Lata, S., Schoehn, G., Jain, A., Pires, R., Piehler, J., Gottlinger, H. G. and Weissenhorn, W. (2008) Helical structures of ESCRT-III are disassembled by VPS4. *Science.* **321**, 1354-1357
- 15 Wollert, T., Wunder, C., Lippincott-Schwartz, J. and Hurley, J. H. (2009) Membrane scission by the ESCRT-III complex. *Nature.* **458**, 172-177
- 16 Weiß, P., Huppert, S. and Kölling, R. (2008) ESCRT-III protein Snf7 mediates high-level expression of the *SUC2* gene via the Rim101 pathway. *Eukaryot Cell.* **7**, 1888-1894
- 17 Hayashi, M., Fukuzawa, T., Sorimachi, H. and Maeda, T. (2005) Constitutive activation of the pH-responsive Rim101 pathway in yeast mutants defective in late steps of the MVB/ESCRT pathway. *Mol. Cell. Biol.* **25**, 9478-9490
- 18 Rothfels, K., Tanny, J. C., Molnar, E., Friesen, H., Commisso, C. and Segall, J. (2005) Components of the ESCRT pathway, *DFG16*, and *YGR122w* are required for *Rim101* to act as a corepressor with Nrg1 at the negative regulatory element of the *DIT1* gene of *Saccharomyces cerevisiae*. *Mol. Cell. Biol.* **25**, 6772-6788
- 19 Xu, W., Smith, F. J., Jr., Subaran, R. and Mitchell, A. P. (2004) Multivesicular body-ESCRT components function in pH response regulation in *Saccharomyces cerevisiae* and *Candida albicans*. *Mol. Biol. Cell.* **15**, 5528-5537
- 20 Kullas, A. L., Li, M. and Davis, D. A. (2004) Snf7p, a component of the ESCRT-III protein complex, is an upstream member of the RIM101 pathway in *Candida albicans*. *Eukaryot Cell.* **3**, 1609-1618
- 21 Li, W. and Mitchell, A. P. (1997) Proteolytic activation of Rim1p, a positive regulator of yeast sporulation and invasive growth. *Genetics.* **145**, 63-73
- 22 Lamb, T. M. and Mitchell, A. P. (2003) The transcription factor Rim101p governs ion tolerance and cell differentiation by direct repression of the regulatory genes *NRG1* and *SMP1* in *Saccharomyces cerevisiae*. *Mol. Cell. Biol.* **23**, 677-686

- 23 Xu, W. and Mitchell, A. P. (2001) Yeast PalA/AIP1/Alix homolog Rim20p associates with a PEST-like region and is required for its proteolytic cleavage. *J. Bacteriol.* **183**, 6917-6923
- 24 Penalva, M. A., Tilburn, J., Bignell, E. and Arst, H. N., Jr. (2008) Ambient pH gene regulation in fungi: making connections. *Trends Microbiol.* **16**, 291-300
- 25 Longtine, M. S., McKenzie, A., 3rd, Demarini, D. J., Shah, N. G., Wach, A., Brachat, A., Philippsen, P. and Pringle, J. R. (1998) Additional modules for versatile and economical PCR-based gene deletion and modification in *Saccharomyces cerevisiae*. *Yeast.* **14**, 953-961
- 26 Gietz, R. D. and Sugino, A. (1988) New yeast-*Escherichia coli* shuttle vectors constructed with in vitro mutagenized yeast genes lacking six-base pair restriction sites. *Gene.* **74**, 527-534
- 27 Kinner, A. and Kölling, R. (2003) The yeast deubiquitinating enzyme Ubp16 is anchored to the outer mitochondrial membrane. *FEBS Lett.* **549**, 135-140
- 28 Kölling, R. and Hollenberg, C. P. (1994) The ABC-transporter Ste6 accumulates in the plasma membrane in a ubiquitinated form in endocytosis mutants. *EMBO J.* **13**, 3261-3271
- 29 Muziol, T., Pineda-Molina, E., Ravelli, R. B., Zamborlini, A., Usami, Y., Göttlinger, H. and Weissenhorn, W. (2006) Structural basis for budding by the ESCRT-III factor CHMP3. *Dev Cell.* **10**, 821-830
- 30 Raymond, C. K., Howald, S. I., Vater, C. A. and Stevens, T. H. (1992) Morphological classification of the yeast vacuolar protein sorting mutants: evidence for a prevacuolar compartment in class E *vps* mutants. *Mol. Biol. Cell.* **3**, 1389-1402
- 31 Lata, S., Roessle, M., Solomons, J., Jamin, M., Gottlinger, H. G., Svergun, D. I. and Weissenhorn, W. (2008) Structural basis for autoinhibition of ESCRT-III CHMP3. *J Mol Biol.* **378**, 818-827
- 32 Saksena, S., Wahlman, J., Teis, D., Johnson, A. E. and Emr, S. D. (2009) Functional reconstitution of ESCRT-III assembly and disassembly. *Cell.* **136**, 97-109
- 33 McCullough, J., Fisher, R. D., Whitby, F. G., Sundquist, W. I. and Hill, C. P. (2008) ALIX-CHMP4 interactions in the human ESCRT pathway. *Proc. Natl. Acad. Sci. USA.* **105**, 7687-7691
- 34 Obita, T., Saksena, S., Ghazi-Tabatabai, S., Gill, D. J., Perisic, O., Emr, S. D. and Williams, R. L. (2007) Structural basis for selective recognition of ESCRT-III by the AAA ATPase Vps4. *Nature.* **449**, 735-739
- 35 Stuchell-Brereton, M. D., Skalicky, J. J., Kieffer, C., Karren, M. A., Ghaffarian, S. and Sundquist, W. I. (2007) ESCRT-III recognition by VPS4 ATPases. *Nature.* **449**, 740-744
- 36 Lupas, A. (1996) Prediction and analysis of coiled-coil structures. *Methods Enzymol.* **266**, 513-525

Figure legends

Figure 1 *SNF7* functions can be separated genetically. (A) Growth phenotypes of *SNF7* mutants. RKY1852 ($\Delta snf7$, panels 1-3) or RKY1854 ($\Delta snf7$ [*CUP1p-STE6-HIS3*], panel 4) were transformed with different plasmids (from top to bottom): pRK861 (WT *SNF7*), YCplac33 (vector control), pRK1048 (*snf7-M3*), pRK1049 (*snf7-M5*). 10-fold serial dilutions of overnight cultures grown in SD/CAS medium were spotted onto different plates and incubated for 3 d under different conditions (from left to right): SD/CAS, 25°C; SD/CAS, 37°C; SD/CAS with 2 % raffinose as sole carbon source (+ 2 μ g/ml antimycin), 25°C; SD + leucine, lysine, tryptophane (= -his), 0.5 mM Cu₂SO₄, 25°C. (B) Distribution of *Snf7* mutations obtained by PCR mutagenesis. The positions of the mutations are indicated by arrows (open box: *Snf7* sequence, dark boxes: predicted α -helical regions). Below: Coiled-coil forming probability determined with the program Macstripe 2.0a1 [36]. (C) Positions of M3 and M5 mutations modeled onto the CHMP3 structure.

Figure 2 Effect of *SNF7* mutations on endocytic trafficking. (A) The turnover of *Ste6* in strain RKY1852 ($\Delta snf7$) transformed with different *SNF7* plasmids was examined by pulse-chase analysis. Cells were labeled with [³⁵S] Trans-label for 15 min and chased with an excess of cold methionine and cysteine for the time intervals indicated. *Ste6* was precipitated from cell extracts with polyclonal antibodies directed against *Ste6*. Precipitated *Ste6* was detected by autoradiography. The calculated *Ste6* half-lives are indicated. (B) Strain RKY1510 ($\Delta snf7$) transformed with plasmid pRK1095 expressing *Ste6*-GFP and with plasmids expressing different *Snf7* variants was grown in SD/CAS medium to exponential phase. Left panels: GFP fluorescence, right panels: DIC image of the yeast cells. (A, B) Plasmids used (from top to bottom): pRK861 (WT *SNF7*), YCplac33 (vector control), pRK1048 (*snf7-M3*), pRK1049 (*snf7-M5*). (C) CPY-sorting was examined in strain RKY1852 ($\Delta snf7$) transformed with different *SNF7* plasmids. Cells were labelled for 10 min with [³⁵S] Trans label and chased with an excess of cold methionine and cysteine for 0 min or 40 min. Carboxypeptidase Y (CPY) was immunoprecipitated from spheroplast (internal, I) fractions (odd numbers) and medium (external, E) fractions (even numbers). The precipitated proteins were analysed by SDS-PAGE and autoradiography. Plasmids used were: (1,2) pRK861 (WT *SNF7*, 0 min chase), (3,4) pRK861 (WT *SNF7*, 40 min chase), (5,6) YCplac33 (vector control), (7,8) pRK1048 (*snf7-M3*), (9,10) pRK1049 (*snf7-M5*). The positions of the different CPY forms are indicated.

Figure 3 Test for *rim* phenotypes. (A) Invertase activity: Cells were grown to exponential phase in SD/CAS medium at 25°C with 5 % glucose and transferred to medium with 0.1 % glucose to induce invertase expression. Invertase activity was determined after 2 h in low glucose medium, as described [16]. The activity with wildtype *SNF7* was set to 100 %; average of three independent experiments (with standard deviations). WT: RKY1852 ($\Delta snf7$)/pRK861 (WT *SNF7*), $\Delta snf7$: RKY1852/YCplac33 (vector), *snf7-M3*: RKY1852/pRK1048, *snf7-M5*: RKY1852/pRK1049. (B) LiCl sensitivity: 10-fold serial dilutions of cell cultures (OD₆₀₀ = 1) were spotted onto SD/CAS plates with (right panel) or without 0.3 M LiCl (left panel) and incubated for 3 d at 25°C. WT: RKY1852/pRK861 $\Delta snf7$: RKY1852/YCplac33, $\Delta rim13$: RKY2102/YCplac33, *snf7-M3*: RKY1852/pRK1048, *snf7-M5*: RKY1852/pRK1049. (C) Cells were grown to exponential phase in SD/CAS medium adjusted to pH 3; half of the culture was adjusted to pH 7 and growth was continued for 30 min before extract preparation. Rim101-3HA was detected by Western blotting with anti-HA antibodies. (1) JD52 (WT, no tag)/YCplac33, (2, 3) RKY2259 ($\Delta rim13$ RIM101-3HA)/YCplac33, (4, 5) RKY2261 ($\Delta snf7$ RIM101-3HA)/YCplac33, (6, 7) RKY2261/pRK861 (WT *SNF7*), (8, 9) RKY2261/pRK1048

(*snf7-M3*), (10, 11) RKY2261/pRK1049 (*snf7-M5*). Even numbers: pH 3, odd numbers: pH 7, asterisk: background band.

Figure 4 Membrane association of Snf7 mutants. Cell extracts of RKY2061 ($\Delta snf7 \Delta vps4$) transformed with different *SNF7* plasmids and grown in SD/CAS medium were fractionated on OptiprepTM flotation gradients. Six fractions (lanes 1-6) were collected from the gradients (lanes 1-3 = float fraction, lanes 4-6 = non-float fraction). In the top three panels, fractions were analyzed by Western blotting with anti-Snf7 antibodies. Plasmids used (from top to bottom): pRK861 (WT *SNF7*), pRK1048 (*snf7-M3*), pRK1049 (*snf7-M5*). In the last three panels, fractions obtained from RKY1852/pRK861 (WT *SNF7*) were analyzed by Western blotting with antibodies directed against different marker proteins, as indicated.

Figure 5 Detection of higher-order Snf7 complexes by cross-linking. Cell extracts were prepared from RKY1852 ($\Delta snf7$) transformed with different *SNF7* plasmids (pRK861: WT *SNF7*, lanes 1-4, pRK1048: *snf7-M3*, lanes 5-8, pRK1049: *snf7-M5*, lanes 9-12) and were treated with increasing concentrations of DSS (0, 1, 2.5, 5 mM). Snf7 reactive bands (marked by arrows, with calculated sizes) were detected by Western blotting with Snf7 antibodies. M = protein standard.

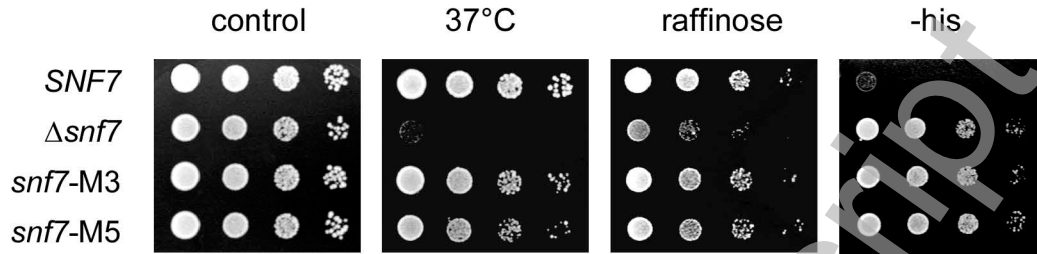
Figure 6 Effect of mutations on Snf7 interactions. The interaction of Snf7 with its interaction partners was examined by co-immunoprecipitation. Different *SNF7* deletion strains expressing 13myc-tagged interaction partners from the chromosomal copy of the corresponding genes were transformed with different *SNF7* plasmids: WT = pRK861, M3 = pRK1048, M5 = pRK1049. Cells were grown in SD/CAS medium adjusted to pH 3. The interaction partners were immunoprecipitated from cell extracts with anti-myc antibodies. The immunoprecipitates were then analyzed for the 13myc-tagged proteins with anti-myc antibodies (lanes 1-3) and for Snf7 with anti-Snf7 antibodies (lanes 5-10) by Western blotting. Strains used (from top to bottom): RKY2107 (Rim13-13myc), RKY2097 (Rim20-13myc), RKY1490 (Snf7-13myc), RKY2401 (Vps20-13myc), RKY2422 (Vps24-13myc), RKY2030 (Bro1-13myc), RKY2126 (Vps4-13myc). I = input (lanes 5, 7, 9), P = immunoprecipitates (lanes 6, 8, 10).

Figure 7 Fractionation of Snf7 and Vps20 by sedimentation. Strain RKY2401 ($\Delta snf7 VPS20-13myc$) transformed with different plasmids was grown to exponential phase in SD/CAS medium adjusted to pH 3. WT Snf7: pRK861 (lanes 1-7), Snf7-M3: pRK1048 (lanes 8-12), Snf7-M5: pRK1049 (lanes 13-17). Cleared cell extracts (Total fraction, lanes 3, 8, 13) were centrifuged at 100,000 g for 1 h and separated into P100 pellet (lanes 4, 9, 14) and S100 supernatant (lanes 5, 10, 15). Equal portions of the fractions were examined by Western blotting with anti-myc antibodies for detection of Vps20-13myc (upper panel) and anti-Snf7 antibodies for detection of Snf7 (lower panel). In addition, the interaction of Snf7 with Vps20-13myc was examined by co-immunoprecipitation. Vps20-13myc was immunoprecipitated from P100 (IP-P100) and S100 fractions (IP-S100) with anti-myc antibodies. The immunoprecipitates (lanes 1, 2, 6, 7, 11, 12, 16, 17) were analyzed for Vps20-13myc with anti-myc antibodies (upper panel) and for Snf7 with anti-Snf7 antibodies (lower panel) by Western blotting. (1, 2) Control immunoprecipitation without anti-myc antibodies.

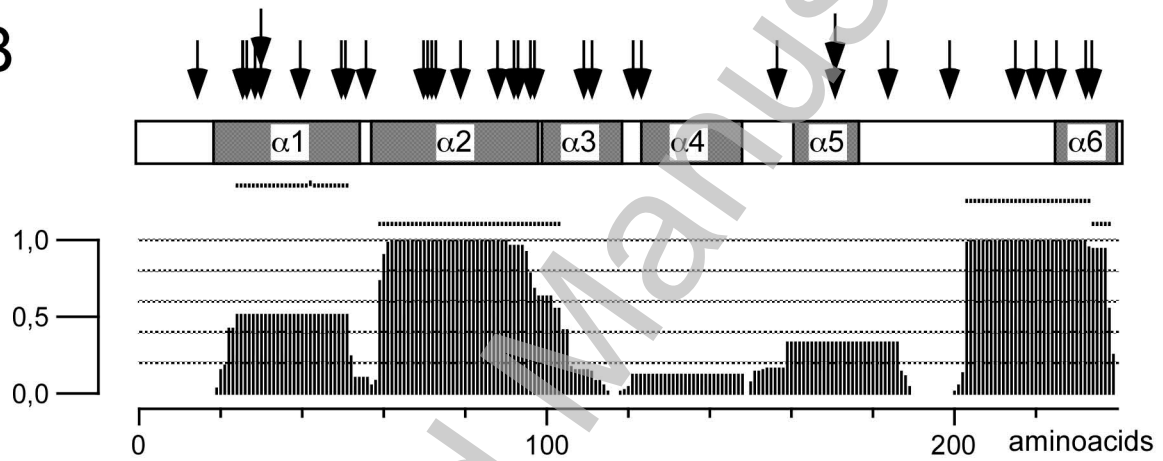
Figure 8 Effect of pH on Snf7 interactions. The interaction of Snf7 with its interaction partners was examined by co-immunoprecipitation. Yeast strains expressing 13myc-tagged interaction partners from the chromosomal copy of the corresponding genes were pre-grown in SD/CAS medium adjusted to pH 3. Half of the culture was adjusted to pH 7, the other half was left untreated. Incubation was continued for 30 min. The interaction partners were

immunoprecipitated from cell extracts with anti-myc antibodies. The immunoprecipitates were then analyzed for the 13myc-tagged proteins with anti-myc antibodies (left panels) and for Snf7 with Snf7 antibodies (right panels). pH 3: lanes 1-3, pH 7: lanes 4 and 5, I = input (lanes 1 and 4), P+ = immunoprecipitate with antibodies (lanes 2 and 5), P- = mock immunoprecipitation, no antibodies (lane 3). Strains used (from top to bottom): RKY2106 (Rim13-13myc), RKY2099 (Rim20-13myc), RKY1633 (Vps20-13myc), RKY2029 (Bro1-13myc), RKY2402 (Vps4-13myc).

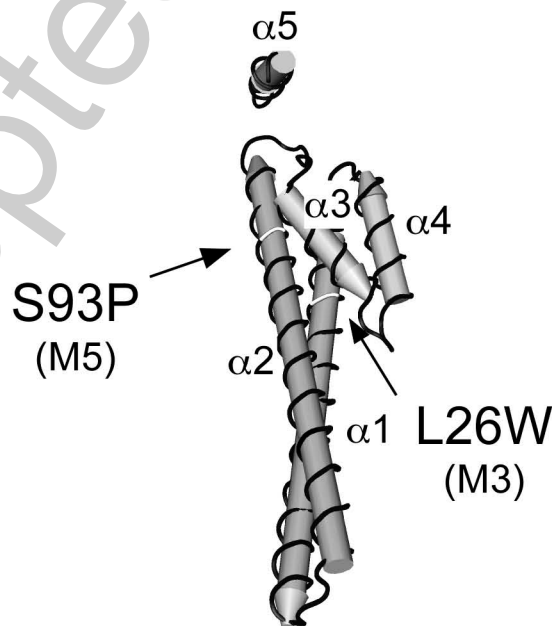
A

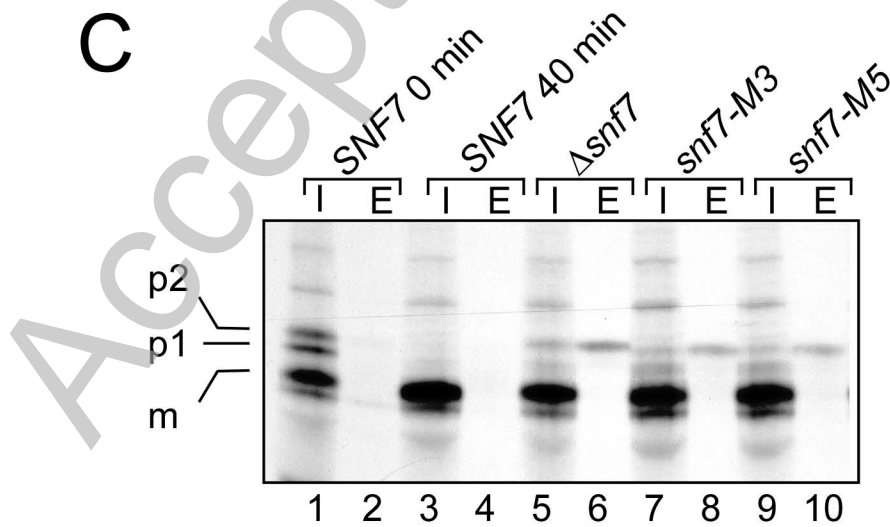
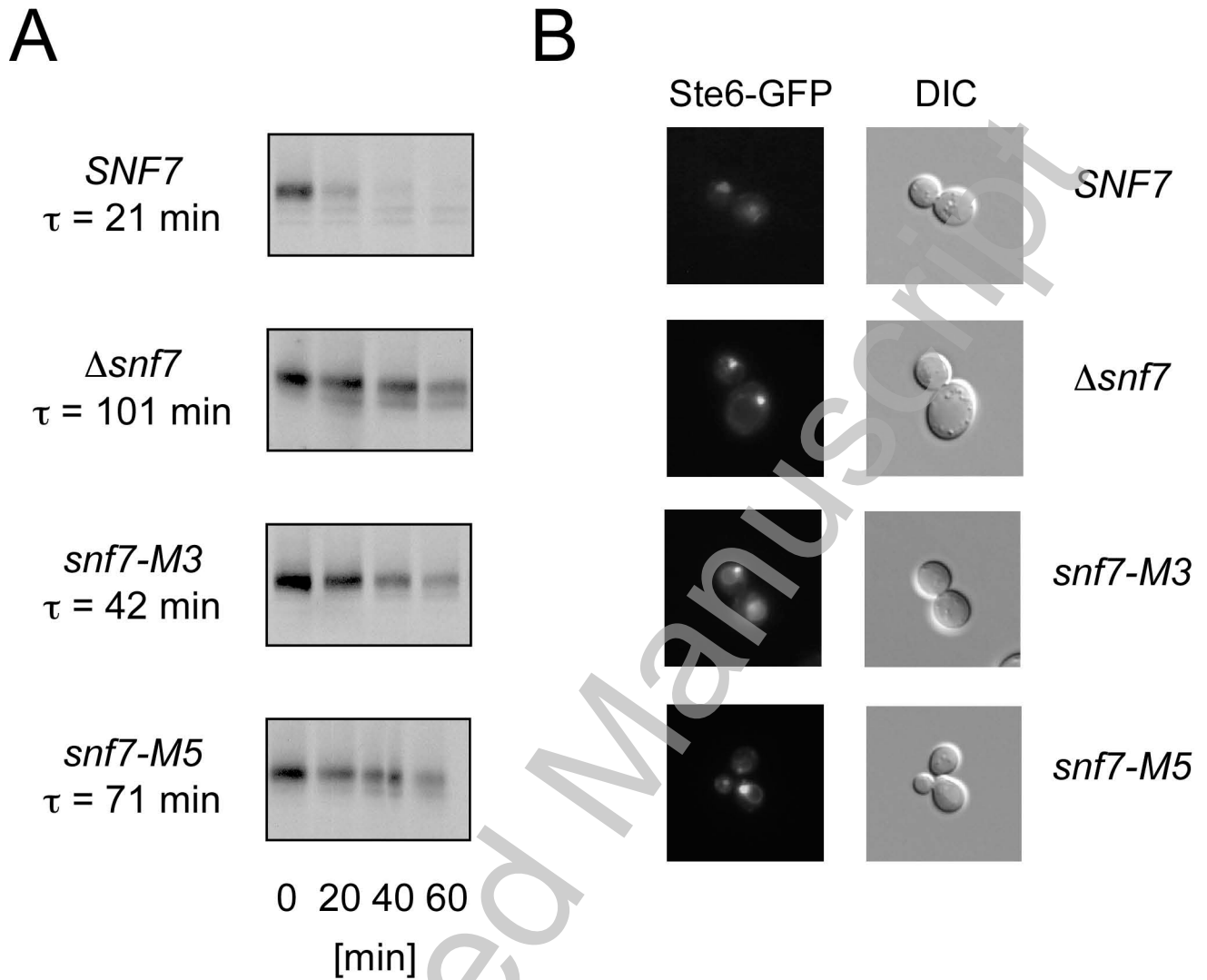


B

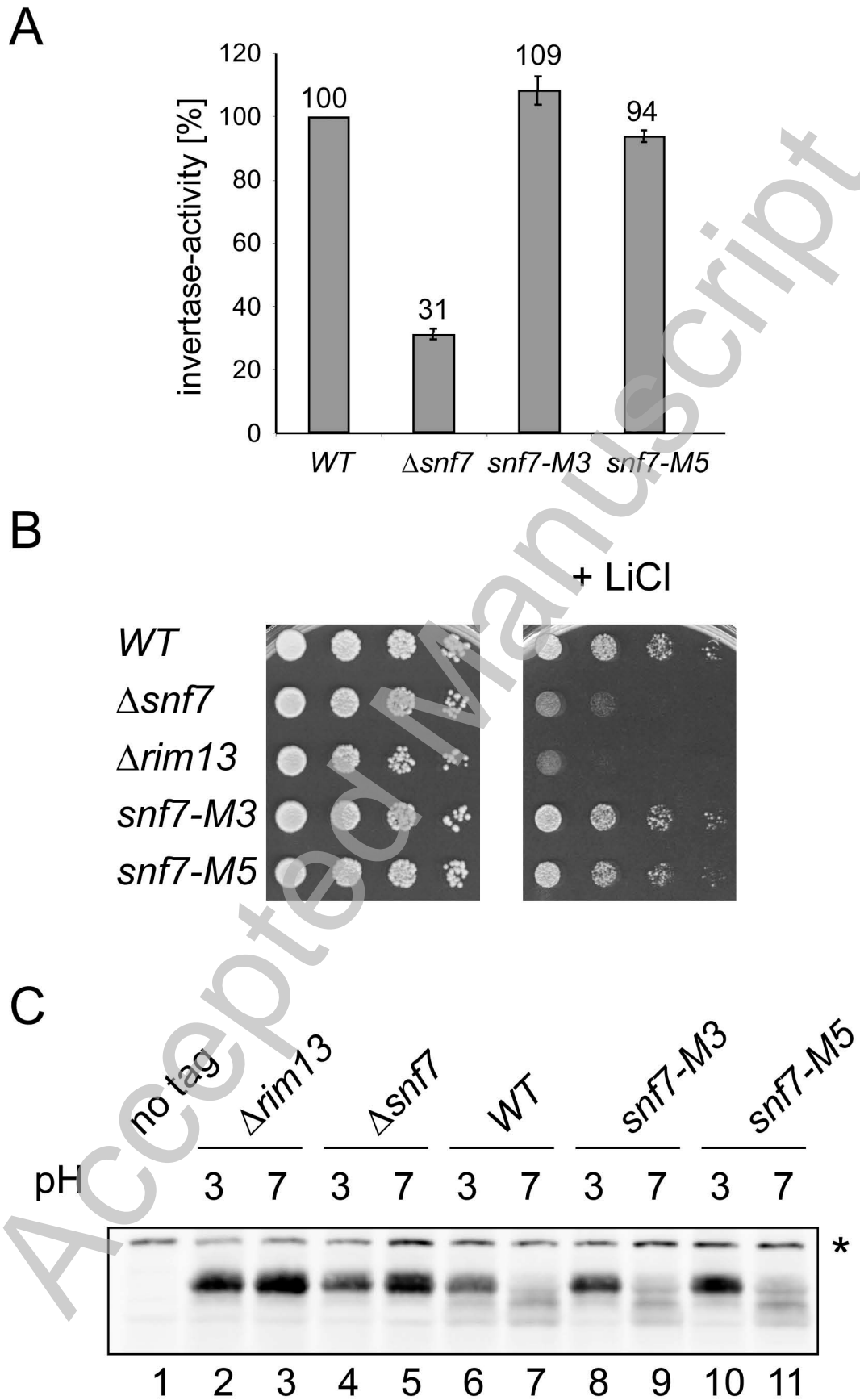


C

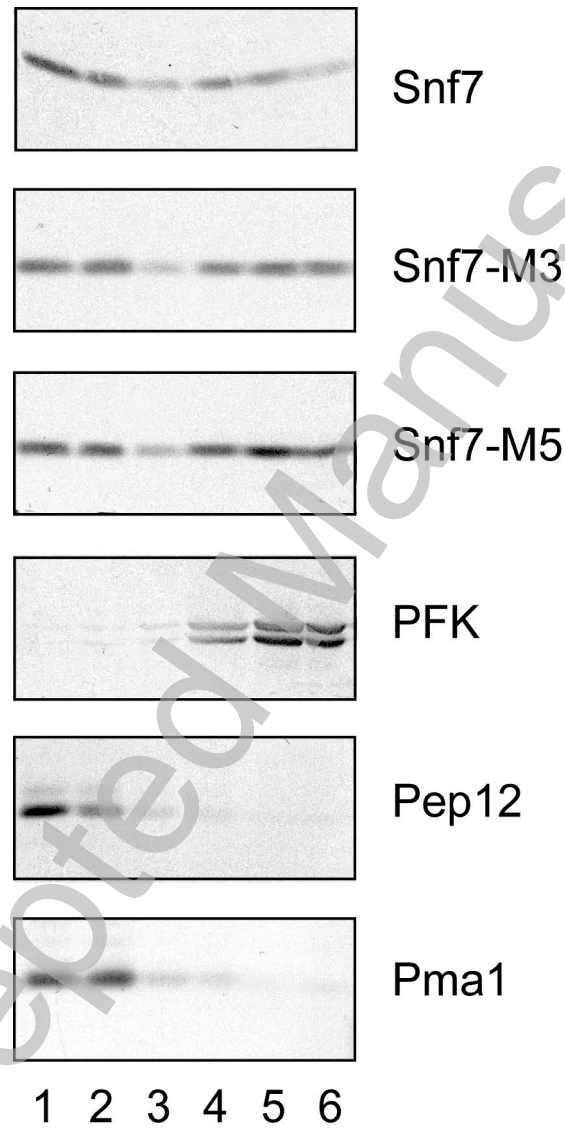


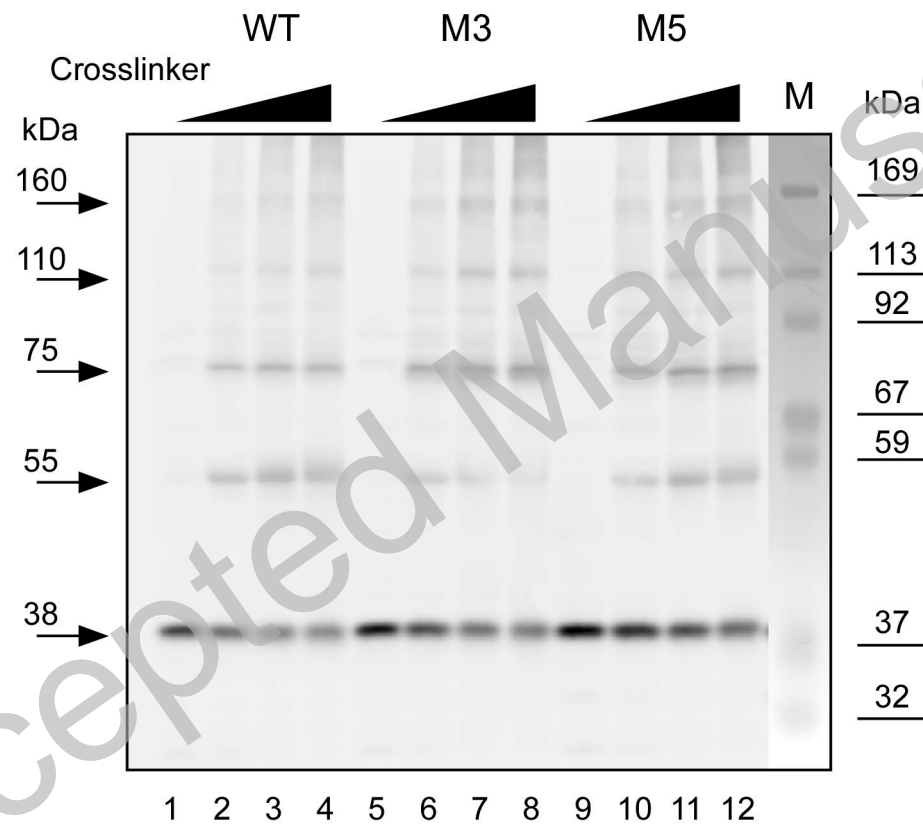


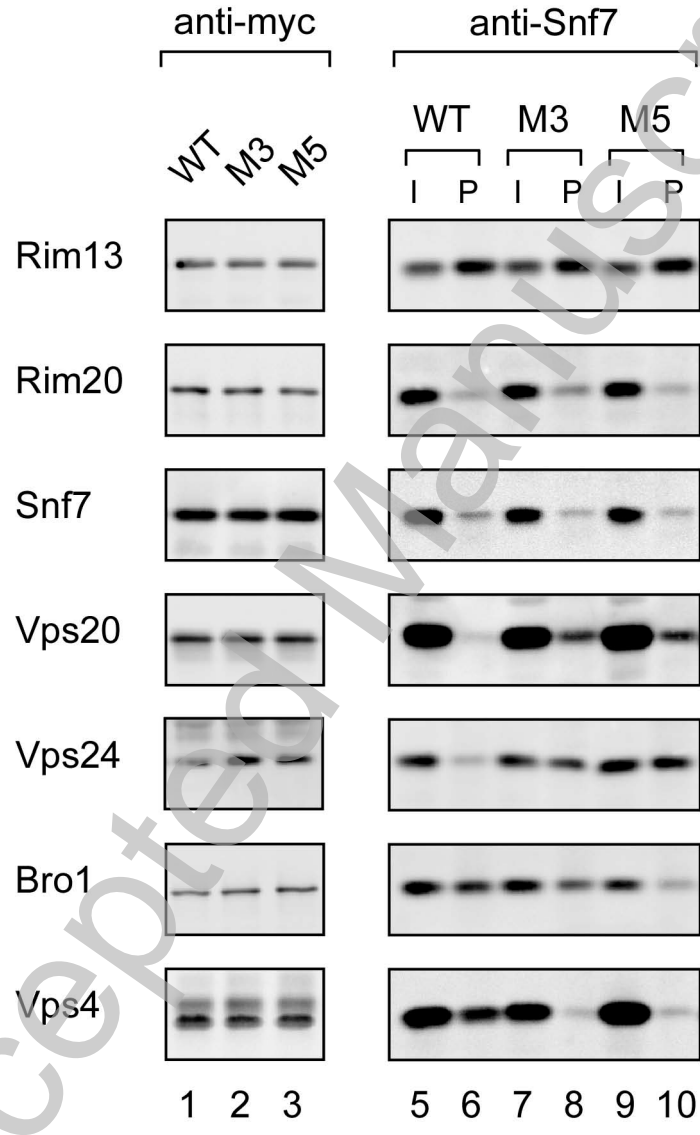
THIS IS NOT THE VERSION OF RECORD - see doi:10.1042/BJ20090957

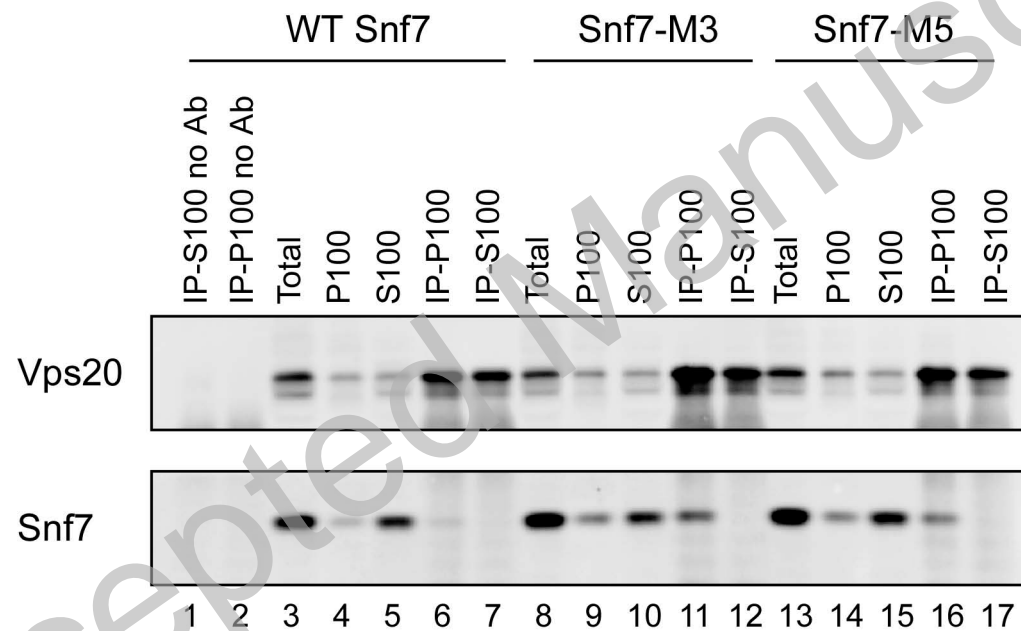


THIS IS NOT THE VERSION OF RECORD - see doi:10.1042/BJ20090957

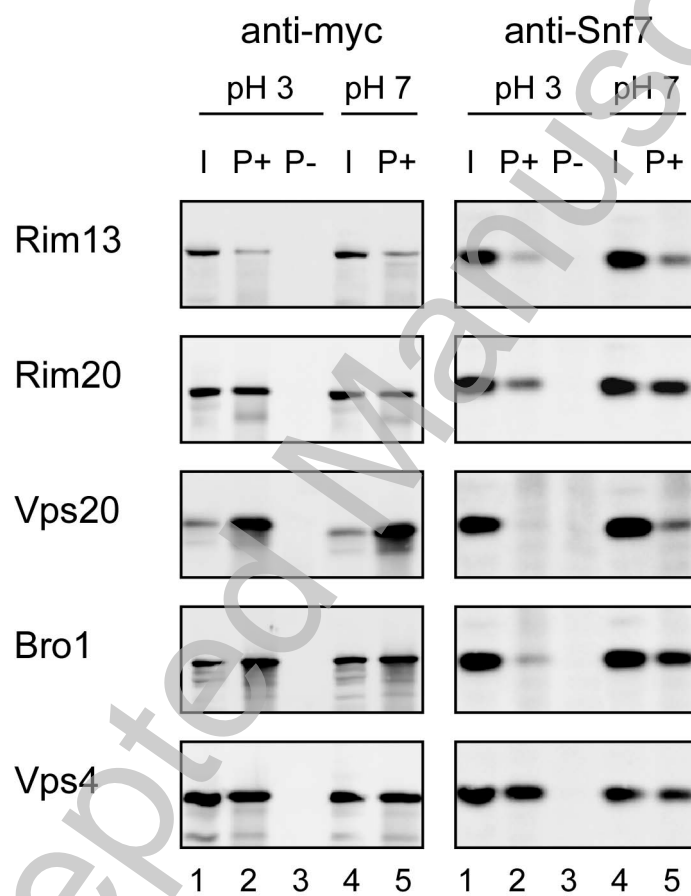








THIS IS NOT THE VERSION OF RECORD - see doi:10.1042/BJ20090957



Tab. 1 Yeast strains

Strain	Genotype	Reference
JD52	<i>MATa his3-Δ200 leu2-3,112 lys2-801 trp1-Δ63 ura3-52</i>	J. Dohmen, Köln
RKY1490	<i>SNF7-13myc::kanMX</i>	this study
RKY1510	<i>Δsnf7::HIS3</i>	this study
RKY1633	<i>VPS20-13myc::HIS3</i>	this study
RKY1852	<i>Δsnf7::TRP1</i>	this study
RKY1854	<i>Δsnf7::TRP1 suc2::[CUP1p-STE6-HIS3]</i>	this study
RKY2029	<i>BRO1-13myc::kanMX</i>	this study
RKY2030	<i>Δsnf7::TRP1 BRO1-13myc::kanMX</i>	this study
RKY2061	<i>Δsnf7::kanMX Δvps4::HIS3</i>	this study
RKY2097	<i>Δsnf7::TRP1 RIM20-13myc::kanMX</i>	this study
RKY2099	<i>RIM20-13myc::kanMX</i>	this study
RKY2102	<i>Δrim13::kanMX</i>	this study
RKY2106	<i>RIM13-13myc::kanMX</i>	this study
RKY2107	<i>Δsnf7::TRP1 RIM13-13myc::kanMX</i>	this study
RKY2126	<i>Δsnf7::TRP1 VPS4-13myc::kanMX</i>	this study
RKY2259	<i>Δrim13::kanMX 3HA-RIM101::HIS3</i>	this study
RKY2261	<i>Δsnf7::kanMX 3HA-RIM101::HIS3</i>	this study
RKY2401	<i>Δsnf7::kanMX VPS20-13myc::HIS3</i>	this study
RKY2402	<i>VPS4-13myc::HIS3</i>	this study
RKY2422	<i>Δsnf7::TRP1 VPS24-13myc::HIS3</i>	this study

Tab. 2 *SNF7* mutants

Mutant	DNA Mutation(s)	Protein Mutation(s)
1	G289A A326G A467G	A97T E109G N156S
2	T89A G331A A367G G655C A671G A696G	I30N A111T I123V E219Q E224G R232K
3	T77G	L26W
4	T692C	L231S
5	T277C	S93P
7	G81T A236C T509C T548C	R27S K79T L170P V183A
8	A208G T641C	K70E V214A
9	T77C T163C	L26S -
11	A86G T89A A198G T274C T592C	H29R I30N - F92S S198P
13	A263G C361T T509C	E88G L121F L170P
24	A120C A149G G151A A166G T288C	L40F E50G A51T T56A -
31	A44G A211G A214G T218C	N15S K71E T72A I73T

Tab. 3 Snf7 Co-immunoprecipitation^a

	WT	M3	M5	n ^b
Rim13	100	91 ± 6	101 ± 8	2
Rim20	100	138 ± 20	75 ± 31	4
Snf7	100	89 ± 22	77 ± 13	3
Vps20	100	754 ± 193	391 ± 29	2
Vps24	100	373 ± 41	382 ± 37	2
Bro1	100	50 ± 25	48 ± 25	6
Vps4	100	38 ± 12	43 ± 6	3

^aratios Snf7 Co-IP signal : Snf7 input signal, WT ratio set to 100, ± standard deviation

^bn = number of experiments

Tab. 4 Membrane fraction (P100) (%)^a

	Snf7	Vps20
WT Snf7	14	33
Snf7-M3	29	42
Snf7-M5	27	46

^atwo experiments were performed with virtually identical results